Quantitative Mapping of Structured Polymeric Systems Using Singular Value Decomposition Analysis of Soft X-ray Images

I. N. Koprinarov, A. P. Hitchcock,* C. T. McCrory,† and R. F. Childs

Department of Chemistry, McMaster University, Hamilton, Ontario L8S 4M1, Canada

Received: August 24, 2001; In Final Form: March 20, 2002

The distribution of poly(acrylic acid) in a microporous polypropylene support membrane has been measured quantitatively by scanning transmission X-ray microscopy (STXM). Singular value decomposition analysis of X-ray microscopy images recorded at carefully selected photon energies was used to obtain quantitative maps of the polypropylene membrane and the poly(acrylic acid) gel, the two components of this system. The sample was studied fully hydrated in order to perform the quantitative mapping when the membrane is the same as in its state of application. Optimum strategies of data acquisition for quantitative X-ray microscopy analysis of radiation sensitive materials are discussed, along with a brief comparison of this technique to alternative methods of mapping the chemical components of structured multicomponent polymeric systems.

1. Introduction

A new class of nanofiltration membrane has been developed at McMaster University. These membranes consist of a water swollen polyelectrolyte gel locked by cross-linking within the pores of a commercially available polyolefin microporous membrane. The fixed charge in the membranes results in a Donnan exclusion of coions.[1] As a result, under pressure driven conditions, the membranes are capable of rejecting salts.[2] These membranes exhibit productivities which exceed currently available nanofiltration membranes.[3]

In terms of understanding the properties of these membranes and further improving their performance it is critical to know the distribution of the polyelectrolyte gels within the microporous host. However, this has proven to be difficult to accomplish using optical microscopy, environmental scanning electron microscopy (ESEM), transmission electron microscopy (TEM), or atomic force microscopy (AFM). In our hands these techniques have either failed to quantitatively distinguish the polyproplylene substrate and the incorporated swollen poly(acrylic acid) gel,[4] or they have inadequate spatial resolution. In this work we demonstrate that soft X-ray spectromicroscopy, combined with appropriate data analysis techniques, can *quantitatively* analyze the composite polymer membrane structure, in particular, determine the spatial distribution of the polyelectrolyte gel relative to the membrane.

Analytical soft X-ray microscopy has been developed and applied to a wide range of materials[5−7] including polymers.[8−10] In this study, a scanning transmission X-ray microscope (STXM)[6,11−13] was used. It provides images with better than 100 nm spatial resolution at variable X-ray energy (160−1260 eV) with a resolving power of more than 3000, corresponding to an energy resolution of about 100 meV in the C 1s region.

The basis for contrast in the images is near edge X-ray absorption fine structure (NEXAFS).[14] Here we have used only carbon 1s spectroscopy but for many polymers other core edges, particularly N 1s and O 1s, can also be used.

The X-ray photoabsorption response of a multicomponent sample is a superposition of the response of each compound present in the column, weighted by its mass absorption coefficient at the photon energy employed, as described by the classical Beer−Lambert optical absorption law. Because of the well-known linear relationship between spectral response (absorption or optical density) and concentration, the spatially resolved X-ray absorption signal can be used for quantitation. To carry out quantitative analyses the NEXAFS spectra of the pure components are recorded and converted to an absolute mass absorption scale by normalizing to the atomic response outside of the fine structure at the core excitation threshold.[15] X-ray images of an heterogeneous sample of unknown local composition and spatial distributions are then recorded at a number of energies and chemical maps are derived by appropriate comparison to linear combinations of the mass absorption coefficients of the constituents taken from the intensity calibrated standards.

Different mathematical methods can be used to obtain component maps from sets of X-ray spectromicroscopy images. A particularly convenient one is called singular value decomposition (SVD).[16,17] Zhang et al.[18] applied SVD to obtain DNA and protein distribution maps from images of sperm cells recorded at a few photon energies, while Buckley and collaborators have applied it to both biological and polymer systems.[19] Complementary to SVD analysis, Osanna and Jacobsen[20] have applied a principle component analysis (PCA) approach to X-ray microscopy. In this procedure the number of components (often called factors in PCA) and their spectral response are not input parameters based on prior knowledge about the sample, but rather are derived in the PCA analysis, and thus are based solely by the statistical properties of the data set. While PCA is very powerful, there can be considerable ambiguity in the determination of the spectral components of the actual chemical constituents from the derived spectral factors, since any reorthogonalization of the statistically determined spectral factors is an equally valid representation of the data. In cases such as the present system, where the chemical constituents are known, and accurate standard spectra are readily measurable, a direct analysis is preferable. In a parallel effort,

* Corresponding author. BIMR, McMaster University, Hamilton, ON L8S 4M1. Phone: (905) 525-9140 ext 24749. E-mail: aph@mcmaster.ca.

† Present address: Osmonics Ltd., 5951 Clearwater Drive, Minnetonka, MN 55343.

10.1021/jp013281l CCC: $22.00
Published on Web 04/30/2002

Hitchcock et al.[21] have demonstrated an alternate to SVD, one which is also based on comparison to standards but which uses a pixel-by-pixel linear regression analysis of image sequences.[22] Each of these mathematical techniques has advantages and disadvantages. This work presents systematically how we use SVD for soft X-ray image analysis, and illustrates its advantages in studies of highly radiation sensitive samples.

Recording sequences of images with fine energy spacing[22] can be very useful for quantitation.[20,21] Indeed, use of a large set of images should improve the quality of the quantitation and has many advantages if the material is poorly characterized as it maximizes the chances to discover previously unknown components. However, even though it is several orders of magnitude less severe than in techniques using electron beams,[23] radiation damage can be a major issue in soft X-ray microscopy, particularly in zone plate techniques such as STXM where the beam is focused and the flux density is very high. In case of easily damaged materials such as polypropylene and poly(acrylic acid), reduction of the X-ray dose to the minimum needed for a meaningful analysis is essential. The impact of radiation damage can be minimized by choosing optimal parameters for data acquisition (fast imaging), and by recording the minimum number of images which provide a meaningful quantitative analysis. For quantitation of an *n*-component system, at least *n* images are needed. This is exactly the regime where SVD, for which only a small number of images are needed, has advantages relative to other approaches. An additional advantage to the SVD approach is that, by reducing the number of images, one can record larger images and so gain a much larger perspective of the sample, while using the same acquisition time. The data presented in this paper is a good example where large image sizes are needed since spatial mapping across a $\sim$70 μm wide membrane was essential to properly address the analytical question. This study was carried out to demonstrate quantitation via SVD in the case of a highly radiation sensitive system, namely a polypropylene water filtration membrane asymmetrically loaded with a poly(acrylic acid) gel. A practical goal was to determine the minimum number of images needed to obtain reliable quantitation. This information allows us to acquire only the data we need without significant damage which could affect the results, particularly in subsequent studies which will map fine details of the interface between the membrane and the poly(acrylic acid) gel.

The membranes studied in this work were prepared by photopolymerizing acrylic acid within the pores of a microporous poly(propylene) host.[4] Under the conditions used the incident light intensity was attenuated through the thickness of the membrane in a manner that was thought could lead to an asymmetric distribution of poly(acrylic acid) across the membrane. The goal of the X-ray microscopy study was to map the distribution of poly(acrylic acid) in the pores across the full width of the polypropylene membrane. This has been done with samples in both the dry state, after embedding in epoxy, as well as in the fully hydrated form which corresponds to the actual state in practical applications. The results of the latter study are presented here. A more detailed presentation of the analytical results from X-ray spectromicroscopy and other techniques for a series of these membranes will be presented elsewhere.

2. Singular Value Decomposition Methodology

When an X-ray beam with energy *E* passes through a material, the intensity *I* is exponentially attenuated, according to

$$I = I_0 e^{-\alpha(E)t} \quad (1)$$

where *t* is the thickness of the material, α is the linear attenuation coefficient at energy *E*, I_0 is the intensity of the initial beam, and *I* is the intensity of the beam transmitted through the sample. Tabulations of X-ray absorption data usually give the energy-dependent mass absorption coefficient $\mu(E)$, where

$$\alpha(E) = \mu(E)\rho \quad (2)$$

and ρ is the density of the material.

For quantitative image analysis, the transmitted signal is converted to an optical density (OD) according to

$$\mathrm{OD}(E) = \ln(I_o/I) \quad (3)$$

The optical density is *linearly* related to the sample properties by

$$\mathrm{OD}(E) = \mu(E)\rho t \quad (4)$$

where $\mu(E)$ is the mass absorption coefficient at X-ray energy *E*, ρ is the density, and *t* is the path through the sample or the sample thickness. If the energy-dependent mass absorption coefficient μ is in cm^2/g and density ρ is in g/cm^3, one obtains the relative path through each of the components in cm.

The OD of a sample containing *j* noninteracting components is then given by

$$\mathrm{OD}(E) = \mu(E)_1\rho_1 t_1 + \mu(E)_2\rho_2 t_2 + \ldots + \mu(E)_j\rho_j t_j \quad (5)$$

where t_j is the "relative path" through each of the constituent with mass absorption coefficient μ_j and density ρ_j. (Note "relative path" is used to encompass cases where the components are not in pure phases, but rather are mixed such that a column of the material has two or more components through its thickness.) If one knows the energy-dependent mass absorption coefficients μ_j and one measures the OD for different energies *E*, one can use linear algebra to convert the images into component maps $\rho t(x,y)$, by solving the above equation system for every pixel (x,y) of the image set. After correction for density, the vertical scale of the derived component maps is the "relative path" of each component that is required to reproduce the total optical density OD at each pixel in the region sampled.

The conversion from measured OD to component thickness can be expressed as a matrix equation:

$$\mathbf{Mx} = \mathbf{d} \quad (6)$$

where **x** is a vector describing the unknown distribution of each component (ρt), **d** are the measured images, converted to OD scale, and **M** is the matrix of the energy-dependent mass absorption coefficients $\mu(E)$ for each component obtained from reference spectra. Equation 6 is a set of *N* linear equations in *N* unknown variables. Theoretically, if one uses as many equations (images at different energies) as there are unknowns (chemical components), then it should be possible to solve the equation system to obtain a unique solution (this assumes the problem is well-conditioned). In the ideal case, having exact coefficients from accurate reference spectra of the *N*-components and *X* noise-free images, it does not matter how many images (equations) we consider for solving the equation system, since the number of linear independent equations will effectively be reduced to N and there will be one unique solution. However, "real" experimental data is a different situation since it always contains noise, often with indeterminate levels of systematic noise. Here, *X* images at different energies, where *X* is more than *N*, result in an overdetermined equation system, which

means that there are more equations than unknowns. There is in general no exact solution vector for over-determined equation systems. The optimum one can achieve is a "close" vector that satisfies in some sense all equations simultaneously. This closeness can be defined in a least-squares sense and may be calculated by minimizing the residual error.[17] The advantage of the singular value decomposition (SVD) procedure is that, once the absorption coefficients for a set of materials and energies are known, one can calculate a priori the matrixes (**U**,**V**) which will optimally invert an overdetermined sampling of energies into the best possible component maps. Specifically[16,17] one solves for **x** by

$$\mathbf{Mx} = (\mathbf{USV}^{\mathrm{T}})\mathbf{x} = \mathbf{d} \qquad \text{and thus} \qquad \mathbf{x} = \mathbf{V}\mu^{-1}\mathbf{U}^{\mathrm{T}}\mathbf{d} \quad (7)$$

where **U** and **V**, are orthogonal matrixes, **S** is the diagonal array of singular values, and superscript T signifies a matrix transpose operation. It can be shown that the SVD solution is the least-squares solution.[16,17]

SVD efficiently solves an overdetermined linear set of equations. The quality of this solution, especially when dealing with experimental data which has noise and systematic errors, would typically be expected to improve as one increases the number of images at different energies used in solving the system. One challenge of developing robust SVD-based image sequence analysis procedures is thus to be sensitive to the tradeoff inherent in the above.

Although the details of the near edge X-ray absorption fine structure provide the basis for distinguishing the components, the reference spectra must be placed on an absolute mass absorption scale in order to achieve quantitative analysis. The mass absorption coefficients are derived from measurements of the NEXAFS spectra of the pure components. In some cases (as in this work), reference spectra can be recorded from regions of the sample known to be pure in one of the components. Practically, spectra are obtained by first recording an energy scan I from the spot of interest and subsequently the incident flux I_o measured with the same detector and optical path but with the sample out of the beam. The spectra are converted to OD by using eq 3 and subsequently converted to a mass absorption scale by matching the signal in the preedge and postedge regions to the sum of tabulated atomic mass absorption coefficients[15] for the elemental composition of the pure component (C_3H_6 for polypropylene and $C_3H_4O_2$ for poly(acrylic acid)).

The result of applying SVD to a sequence of X-ray mages is a set of component maps, each of which is a plot of the density−thickness product (density-weighted "relative path") for a given component. Accordingly, after correction for density, these maps provide component distributions in the thin section, within the uncertainties of the data and the method.

For most samples ~100 nm g cm^{-3} is an optimal thickness for C 1s STXM imaging since this gives maximum optical densities of 1−2 OD units. Too thin or too thick samples give noisy or saturated spectra, which make it difficult or impossible to perform a quantitative analysis. The uncertainties in the results of this quantitative analysis are determined by a number of factors. In addition to the statistical limits of the images and reference spectra, there are systematic errors associated with: the accuracy of the calculated mass absorption coefficients;[15] knowledge of the density of a component in the sample environment; absorption saturation distortion; contributions from the halo of the incident beam,[24] and the influence of higher order spectral contamination. Since the SVD mathematical procedure works in all cases, if the reference spectral information contained in the input matrix **M** are not appropriate for the problem at hand (for example, due to chemical difference between reference and sample) then erroneous chemical maps may result.

3. Experimental Section

Sample Synthesis and Preparation. The porous substrate used in this study was a poly(proplylene) [PP] microfiltration membrane (3M Company) produced by a thermally induced phase separation process.[25] The PP substrate had a bubble point diameter of 0.57 μm with a porosity of 84.5% and average thickness of 72 μm. The porous membrane was loaded with lightly cross-linked poly(acrylic acid) in a manner similar to that described in Winnik et al..[4]

A cross section of the wet membrane was frozen at −120 °C and cryomicrotomed, to approximately 300 nm thickness. While frozen, the microtomed section was laid flat on a (250 μm × 250 μm Si_3N_4 window and a second Si_3N_4 window was placed on top, in registry. The sample was warmed to room temperature to create the wet sample, which was analyzed at room temperature. The C 1s images were recorded with beam line 7.0 STXM at the Advanced Light Source (ALS).[12,13] The transmitted X-ray photon flux was measured on single photon counting basis using a scintillation converter and a high-performance photomultiplier tube (Hamamatsu 647P). To avoid any absorption by the air, the microscope chamber is completely filled with helium at atmosphere pressure after the sample is installed. Typical count rates were 2×10^7 photons/s transmitted through the helium at 300 eV, with the ALS storage ring running at 1.9 eV, 400 mA. Counting periods (dwell times) of 0.2 ms per pixel were used for analytical imaging. Currently the best spatial resolution of the microscope is about 100 nm, mainly limited by mechanical vibration, rather than the zone plate, which has a diffraction-limited resolution of about 50 nm. The entrance and exit slits of the monochromator were set to obtain an energy resolution of about 100 meV in the carbon 1s region ($E/\Delta E \sim 3000$).

Images were recorded at selected energies through the carbon edge region. Images at a photon energy particularly sensitive to radiation damage (289 eV) were recorded after each image sequence to monitor damage. Postacquisition image alignment[22] was used to correct for drift of the field of view associated with lateral run-out of the zone plate as it is moved along the optical axis to maintain focus.

The reference mass absorption coefficient signal for the polyacrylic gel was derived from regions of a separately recorded image sequence as well as from the set of images recorded for this SVD analysis. As we show below, the latter is preferred for quantitative analysis of the [poly(acrylic acid) gel distribution. The reference mass absorption coefficient signal for polypropylene was obtained from a spectrum of pure polypropylene recorded at the NSLS STXM.[26] The incident flux signal used to convert the measured transmission intensity to optical density was recorded through the water layer and the two Si_3N_4 windows in a region of the wet cell structure adjacent to the membrane. Thus we do not need to explicitly account for water or the Si_3N_4 window absorption in the quantitative analysis.

4. Results

Figure 1a is a STXM image at 300 eV of a microtomed section of the wet polypropylene membrane section sandwiched between two Si_3N_4 windows. Images similar to this were recorded at 11 different energies (from 287.6 to 289 eV in 0.2 eV steps and from 289 to 295 eV in 1.5 eV steps) from the

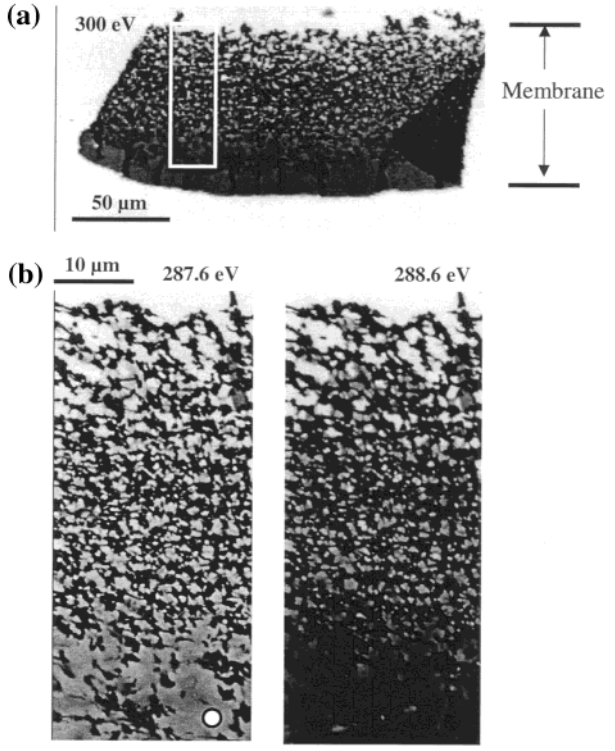

Figure 1. (a) Transmission mode STXM image at 300 eV of a thin section (~300 nm) of a polypropylene membrane loaded with poly(acrylic acid) gel and sandwiched wet between two Si_3N_4 windows. The polypropylene membrane is the very dark structure while the acrylic acid gel is the lighter gray signal which is nonuniform across the membrane. (b) Images at 287.6 and 288.6 eV of the sub-region indicated in (a). Note the changes in contrast due to the different absorption properties of the two polymers at the different photon energies. The poly(acrylic acid) signal used to obtain the reference mass absorption coefficients was obtained from the area marked by the white dot. All three gray scale images are transmitted light signal.

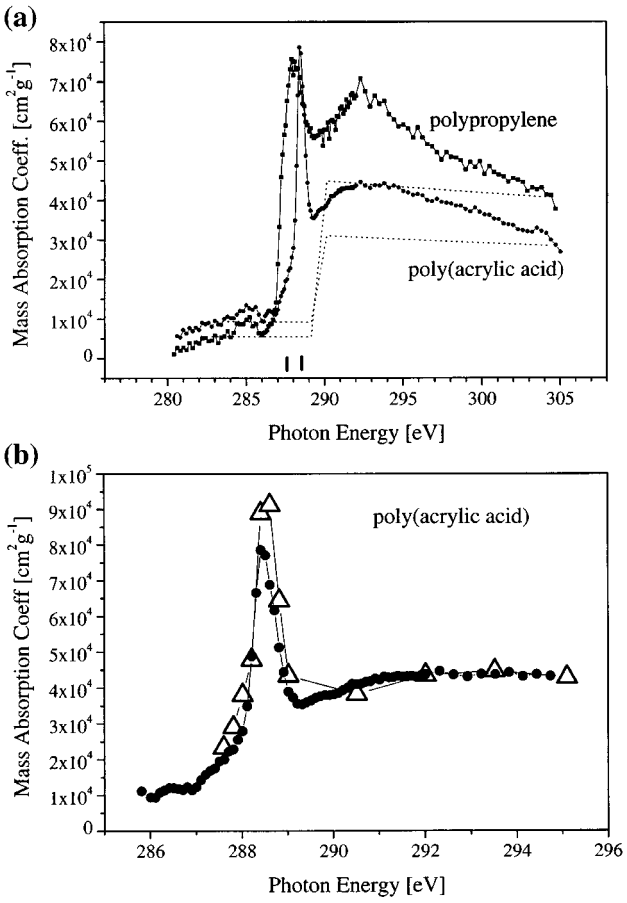

Figure 2. (a) NEXAFS spectra of poly(acrylic acid) gel and polypropylene obtained from a fine mesh image sequence (each point is extracted from an image) compared to the spectrum of polypropylene, recorded on the pure material. The spectra are plotted on quantitative mass absorption scales. The dashed line is the calculated elemental absorption of the pure materials,[15] which was used to convert each spectrum to absolute mass absorption units. (b) Comparison of the poly(acrylic acid) spectrum in Figure 2a (solid dots) to the spectrum obtained from only 11 images (triangles). Accumulated radiation damage has reduced the intensity of the carbonyl resonance in the finely sampled spectrum.

sub-region indicated. Two of these images (recorded at 287.6 and 288.6 eV) are plotted in Figure 1b to illustrate the large change in contrast due to the different absorption properties of the two polymers at these two photon energies.

The spectroscopic basis for distinguishing the polymer components is presented in Figure 2a, which plots the C 1s NEXAFS spectra of polypropylene and poly(acrylic acid) gel in mass absorption units. The figure also plots the calculated elemental absorption curves[15] which were used to convert both spectra to mass absorption units. (Note that the edge positions of the elemental absorption curves have been adjusted to 290 eV, which is a more reasonable value based on the NEXAFS spectroscopy than the 285 eV position tabulated in the Henke database). The polypropylene spectrum is dominated by a strong broad transition at 287.9 eV which is attributed to C 1s $\rightarrow \sigma^*_{C-H}$ transitions. The broad peak at 292 eV is associated with σ^*_{C-C} resonances. The C 1s spectrum of the acrylic acid gel is dominated by the C 1s$\rightarrow\pi^*_{C=O}$ transition at 288.5 eV. There are also signals at ~288 eV (shoulder), 292 eV and ~305 eV, corresponding to σ^*_{C-H}, σ^*_{C-C}, and $\sigma^*_{C=O}$ resonances.

The poly(acrylic acid) spectrum plotted in Figure 2a was obtained from an image sequence, which was recorded with a fine energy spacing (the signal at each data point was extracted from an image). Figure 2b compares the acrylic acid NEXAFS spectrum with the signals obtained from the 11 images analyzed by SVD in this paper. It is clear from the difference in the intensity at the 288.5 eV $\pi^*_{C=O}$ signal that, when the reference spectrum was recorded using the fine spacing image sequence, the acrylic acid was damaged over the period prior to acquiring the carbonyl signal. The distortion of the spectral feature due to the accumulated damage raises questions about the suitability of the fully sampled spectra as reference spectra for quantitation. Therefore, the "spectrum" of poly(acrylic acid) extracted from the 11 images was the basis for the reference mass absorption coefficients used for the quantitative analysis.

Figure 3 compares polypropylene and poly(acrylic acid) component maps derived by applying SVD to two different sets of images. The results on the right are derived from all 11 images while those on the left were derived using only 2 images, those at 287.6 and 288.6 eV (Figure 1b), selected for strong chemical contrast. Each map represents the spatial distribution of a component with the vertical intensity scale giving the "relative path" in nm cm^3 g^{-1}. The derived component maps are similar for both procedures although the two-image component maps show lower contrast and contain a somewhat larger number of physically meaningless negative values. Quantitatively, the polypropylene map from two-images has 18% negative pixels, while that from 11-images has 14% negative pixels. The two-image and 11-image poly(acrylic acid) maps both have 8% negative pixels. Relative to the noise in the

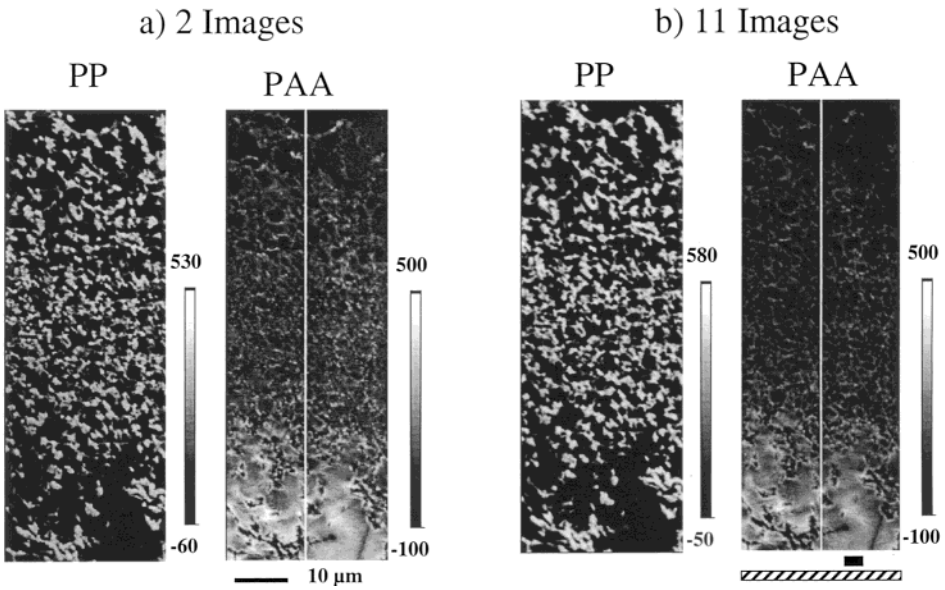

Figure 3. Polypropylene(PP) and poly(acrylic acid) (PAA) component maps derived by applying SVD to (a) only two images (at 287.6 and 288.6 eV) and (b) all 11 images. The vertical scales are relative path (thickness × density). The bars below the PAA map in Figure 3b are the regions for which the averaged poly(acrylic acid) gel thickness across the membrane are plotted in Figure 5.

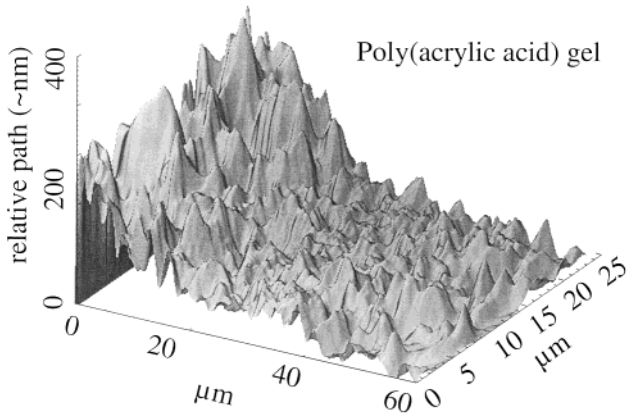

Figure 4. The poly(acrylic acid) component map derived from SVD of 11-images, 15-point-smoothed, and presented as a three-dimensional plot. This clearly shows the pronounced gradient across the membrane. In contrast, the distribution of poly(acrylic acid) in individual pores at a given position across the gradient is relatively a uniform.

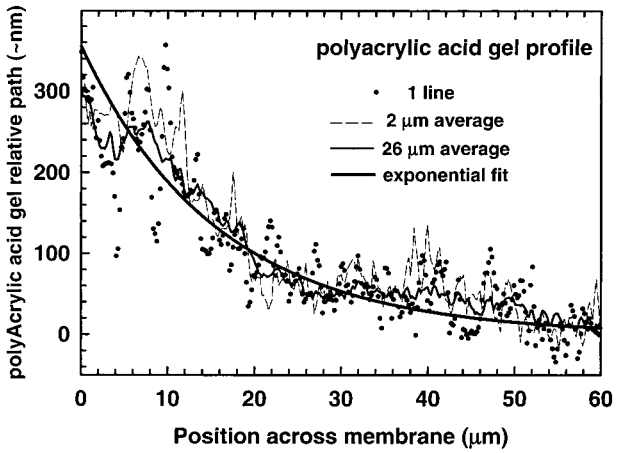

Figure 5. Profiles of the poly(acrylic acid) gel determined from a single vertical line (points), average over 2 μm (dashed line), and averaged over the full 26 μm width sampled (dashed line). See bar in Figure 3b for location of the profiles. The thick solid line is a single-exponential fit to the average over the full width. The decay constant is -0.07 μm^{-1}.

original images, both the two- and 11-image derived component maps have much lower noise, a common result of this type of analysis.

Both SVD analyses presented in Figure 3 clearly show the poly(acrylic acid) is distributed asymmetrically across this membrane. In contrast the polypropylene distribution is relatively uniform, aside from the bottom region of the imaged area where the polypropylene pores have been enlarged presumably due to the swelling of the cross-linked poly(acrylic acid) gel. To further evaluate the two-dimensional spatial distribution of the gel in the polypropylene membrane and to measure the gradient quantitatively, the 11-image component map of poly(acrylic acid) was smoothed (15 points) and is presented in Figure 4 as a three-dimensional plot. This presentation clearly shows the pronounced gradient across this membrane. Inspection of the poly(acrylic acid) distribution within single pores indicates that it is relatively uniform, at least at the spatial sampling used in this work (200 nm). The asymmetric loading of the gel in the membrane occurs on a spatial scale considerably coarser than the average pore size.

In order to use these measurements to help optimize synthetic routes to controlling the asymmetric loading of the membrane, it is useful to *quantitatively* characterize the distribution of the gel across the membrane. Given the photochemical generation of the asymmetric loading, it is appropriate to model this distribution with a combination of an exponential fit (to match to the optical absorption process involved) and a constant (to account for any thermal or other poylmerization mechanism). The result of this analysis applied to the gel component map derived from the 11-image SVD is presented as Figure 5. In order to reduce the sensitivity to the random distribution of the polypropylene pores, the analysis is performed on an average across the full width sampled, although profiles for a single line and a 2 μm width are also plotted (the regions sampled are indicated in Figure 3). The constant term is essentially zero while the exponential fall off has a constant of 0.07 μm^{-1}.

In the case of damageable materials, the optimum strategy is a balance between a larger number of energies, which allow better separation of similar components, and a strict limit on

the number of images to minimize damage. Comparison of the two-energy and 11-energy SVD derived component maps shows that, if the energies for images are selected carefully, then it is possible to obtain quite reasonable results even with the absolute minimum number of images. This means that, at least in this system, it is possible to use an acquisition strategy which truly minimizes radiation damage. It can be seen that if the spectral signatures of both components are sufficiently different, a number of images that is the same or just a bit larger than the number of components is sufficient for good results.

5. Discussion

The accuracy of the result is dependent on the accuracy of the spectral signatures of the individual components. In general it will also strongly depend on the degree to which the reference spectra correspond to the material actually studied, although the partial use of internal standards in this case minimizes that source of uncertainty. The meaningfulness of the SVD approach should not be overestimated, nor should the technique be applied blindly. It has to be applied carefully and used only to extend in a quantitative sense, results which can be ascertained qualitatively from the energy dependence of the images. Generally, the best results are achieved when NEXAFS spectra are extracted from the same image sequence (internal standard method). If this is not possible because regions of pure material could not be found or identified as such, it is recommended that the spectra are obtained at least with the same instrument from carefully chosen pure materials since the final quantitative results strongly depend on the degree to which the reference spectra correspond to the material actually studied.

The results presented for this single membrane illustrate a number of important advantages of the STXM technique for quantitative chemical mapping relative to other approaches. First, it is important to be able to study the material in the wet state since it is the distribution of the poly(acrylic acid) gel in the wet state which is critical to filtration membrane performance in actual applications. There is good reason to suspect this distribution may differ between initially prepared, dried, and rehydrated gel-loaded membranes. Electron beam based microscopies, while providing potentially superior spatial resolution, cannot carry out studies in the presence of liquid water. In addition, the ability to study the wet sample meant that intrusive sample preparation such as epoxy filling of the pores prior to microtomy could be avoided. In many cases epoxy impregnation radically alters soft, readily deformable materials such as membranes. Significant differences were found between this result for the wet membrane and that for the corresponding sample in the dry, epoxy-filled state (not shown). These differences are attributed in large measure to artifacts in the preparation of the epoxy-filled sample. Second, the ability to monitor radiation damage through highly sensitive absorption spectroscopy, not just mass loss effects, and to acquire data with negligible sample damage is a critical advantage, since the quantitation is based on the strength of the 288.5 eV poly(acrylic acid) $\pi^*_{C=O}$ peak which changes most rapidly with damage. Third, the technique is able to sample the full width of the membrane at high spatial resolution in an efficient manner. This is an advantage relative to scanning probe techniques which have difficulties providing a large field of view. Fourth, the component map of the gel is based on a balanced sampling through the full thickness of the sample section ($\sim$0.3 μm), and thus the derived gel distribution is representative of the full membrane, not just the top or bottom portion. This is in contrast to highly surface sensitive techniques such as X-ray photoelectron spectroscopy (XPS) or AFM, which are only able to sample the outermost surface of a sample. Given the extremely heterogeneous porous nature of these membranes, this is a critical advantage. Finally, and perhaps most important, the quantitative chemical analysis is based on the intrinsic spectroscopic properties of the constituents of the sample, and does not require any fluorescence or heavy atom labeling to achieve differentiation. The latter approaches, while certainly very powerful, raise questions about potential sample modification from the labeling chemistry.

We have also examined these membranes using other techniques. In ESEM studies it was found that the poly(acrylic acid) gels collapsed against the poly(propylene) host and as a result it was not possible to distinguish the polypropylene from the poly(acrylic acid). This collapse occurred even in the presence of water vapor in the sample chamber. To probe the distribution of poly(acrylic acid) through the thickness of a membrane, energy-dispersive X-ray analysis (EDX) was applied to microtomed cross-sections of membranes in which the incorporated acid was in the form of heavy atom salts. This approach was able to give an indication of distribution but not with the type of detail which is available with this present technique. It should be noted that these membranes are damaged by the high energy electron beams used for ESEM and EDX, especially at high magnification. The samples must be gold coated for high resolution images, and presumably the gold coating could modify the membranes. Confocal microscopy and AFM results have not yet been obtained to our satisfaction, and even with optimal results, we expect to have concerns with results from both of these techniques. The spatial resolution of confocal microscopy is lower than STXM and the chemical components would not be distinguished without fluorescence labeling. Even with fluorescence labeling of the poly(acrylic acid) the water filled gaps and the polypropylene might both be transparent, resulting in ambiguity of the orientation of the poly(acrylic acid) relative to the membrane support. AFM would only give surface not cross-sectional imaging and is difficult to apply to the rough surface of these porous membranes.

In this paper we have emphasized the technique and the SVD methodology. In a subsequent publication we will compare the gel distribution to models of the photochemical method for generating the asymmetry and discuss the role of these results in the optimization of membrane performance. Finally we note that new information will be accessible when measurements are made at the limits of existing spatial resolution of STXM ($\sim$50 nm) or, even better, with the improved STXM spatial resolution which will result from improved focusing optics (zone plates providing 25 nm performance have been demonstrated recently[27]). It will be possible to map the detailed morphology of the poly(acrylic acid) gel within individual pores which will provide useful information about the gel−membrane and gel−water interfaces. These capabilities will be a significant expansion of the analytical information relative to the distribution across the full membrane that has been illustrated here. They could provide extremely valuable information to guide further improvements in membrane performance. Clearly, analytical soft X-ray microscopy is a very general technique applicable to virtually all classes of materials.

6. Summary

Singular value decomposition of sets of images recorded at carefully selected photon energies was successfully applied to quantify the spatial distributions of poly(acrylic acid) in a polypropylene membrane. Optimum strategies of data acquisi-

tion and analysis for damageable materials were discussed. The component maps reveal for the particular sample studied there is a systematic gradient in the poly(acrylic acid) gel across the ~70 μm thick polypropylene membrane.

Acknowledgment. Research funded by NSERC (Canada), 3M Canada, and the Canada Research chair program. The ALS STXM was developed by T. Warwick (ALS), B.P. Tonner (UWM), and collaborators. Zone plates at ALS were provided by Eric Anderson of CXRO, LBNL. The Advanced Light Source is supported by the Director, Office of Science, Office of Basic Energy Sciences, Materials Sciences Division, of the U.S. Department of Energy under Contract No. DE-AC03-76SF00098 at Lawrence Berkeley National Laboratory.

References and Notes

(1) Mika, A. M.; Childs, R. F.; Dickson, J. M.; McCarry, B. E.; Gagnon, D. R. *J. Membr. Sci.* **1995**, *108*, 37−56. Mika, A. M.; Childs, R. F.; Dickson, J. M.; McCarry, B. E.; Gagnon, D. R. *J. Membr. Sci.* **1997**, *135*, 81−92. Mika, A. M.; Childs, R. F.; West, M.; Lott, J. N. A. *J. Membr. Sci.* **1997**, *136*, 221−232.

(2) Pandey, A. K.; McCrory, C. T. C.; Mouton, S.; Mika, A. M.; Dickson, J. M.; Childs, R. F. *Separation and Purification Technology*, **2000**, March 30. In press.

(3) Mika, A. M.; Childs, R. F.; Dickson, J. M. *Desalination* **1999**, *121*, 149.

(4) Winnik, F. M.; Morneau, A.; Mika, A. M.; Childs, R. F.; Roig, A.; Molins, E.; Ziolo, R. F. *Can. J. Chem.* **1998**, *76*, 10.

(5) Kirz, J.; Jacobsen, C.; Howells, M. *Q. Rev. Biophys*. **1995**, *28*, 33.

(6) Ade, H. In *Experimental Methods In The Physical Sciences*; J. A. R. Samson, J. A. R., Ederer, D. L., Eds., Academic Press: New York, 1998; Vol. 32, p 225.

(7) Ade, H.; Urquhart, S. G. In *Chemical Applications of Synchrotron Radiation*; Sham, T. K., Ed.; World Scientific Publishing: River Edge, NJ. In press.

(8) Ade, H.; Zhang, X.; Cameron, S.; Costello, C.; Kirz, J.; Williams, S. *Science* **1992,** *258*, 972. Ade, H.; Hsiao, B. *Science* **1992**, *262*, 1427.

(9) Ade, H.; Smith, A. P.; Cameron, S.; Cieslinski, R.; Costello, C.; Hsiao, B.; Mitchell, G. E. Rightor, E. G. *Polymer* **1995**, *36*, 1843.

(10) Smith, A. P.; Ade, H. *Appl. Phys. Lett.* **1996** *69*, 3833,

(11) Ade, H.; Smith, A. P.; Zhang, H.; Winn, B.; Kirz, J.; Rightor, E. G.; Hitchcock, A. P. *J. Electron Spectrosc.* **1997**, *84*, 53.

(12) Warwick, T.; Padmore, H.; Ade, H.; Hitchcock, A. P.; Rightor, E. G.; Tonner, B. P. *J. Electron Spectrosc.* **1997** *84*, 85.

(13) Warwick, T.; Franck, K.; Kortwight, J. B.; Meigs, G.; Moronne, M.; Myneni, S.; Rotenberg, E.; Seal, S.; Steele, W. F.; Ade, H.; Garcia, A.; Cerasari, S.; Denlinger, J.; Hayakawa, S.; Hitchcock, A. P.; Tyliszczak, T.; Rightor, E. G.; Shin, H.-J. Tonner, B. P. *Rev. Sci. Instrum.* **1998**, *69***,** 2964.

(14) Stöhr, J. *NEXAFS Spectroscopy*; Springer-Verlag: Berlin, 1992.

(15) Henke, B. L.; Gullikson, E. M. Davis, J. C. *At. Nucl. Data Tables* **1993**, *54*, 181. See also http://www-cxro.lbl.gov/optical_constants/.

(16) Strang, G. *Linear Algebra and Its Applications*; Harcourt Brace Jovanovich: San Diego, 1988

(17) Press, W. H.; et al. *Numerical Recipes in C: The Art of Scientific Computing*; Cambridge University Press: Cambridge, 1992.

(18) Zhang, X.; Balhorn, R.; Mazrimas, J.; Kirz, J. *J. Struct. Biol.* **1996**, *116*, 335.

(19) Buckley, C. J.; Khaleque, N.; Bellamy, S. J.; Robins, M.; Zhang, X. *J. Phys. IV* C2 **1998**, *7***,** 83.

(20) Osanna, A.; Jacobsen, C. X-ray Microscopy. In *Proceedings of the AIP Conference*; Meyer-Ilse, W., Warwick, T., Attwood, D., Eds.; American Institute of Physics: Woodbury, NY, 2000; Vol. 507, p 350.

(21) Hitchcock, A. P.; Koprinarov, I.; Pecher, K.; Kneedler, E. M. In preparation.

(22) Jacobsen, C.; Wirick, S.; Flynn, G.; Zimba, C. *J. Microscopy* **2000**, *197*, 173.

(23) Rightor, E. G.; Hitchcock, A. P.; Ade, H.; Leapman, R. D.; Urquhart, S. G.; Smith, A. P.; Mitchell, G. E.; Fischer, D.; Shin, H. J.; Warwick, T. *J. Phys. Chem. B* **1997**, *101*, 1950.

(24) Hitchcock, A. P.; Koprinarov, I.; Tyliszczak, T.; Rightor, E. G.; Mitchell, G. E.; Dineen, M. T.; Hayes, F.; Lidy, W.; Priester, R. D.; Urquhart, S. G.; Smith, A. P.; Ade, H. *Ultramicroscopy* **2001**, *88*, 33.

(25) Lloyd, D. R.; Kinzer, K. E.; Tseng, H. S., *J. Membr. Sci.* **1990**, *52***,** 239.

(26) Urquhart, S. G. Private communication

(27) Meyer-Isle, W.; Denbaux, G.; Johnson, L. E.; Bates, W.; Lucero, A.; Anderson, E. H. X-ray Microscopy. In *Proceedings of the AIP Conference*; Meyer-Ilse, W., Warwick, T., Attwood, D., Eds.; American Institute of Physics: Woodbury, NY, 2000; Vol. 507, p 129.